Department of Electrical and Computer Engineering

ELECTENG 721 Radio Systems
ELECTENG 737 Advanced Radio Systems

Antennas

Andrew Austin

Part A—Wire Antennas

Wire antennas are the oldest and most commonly used of all antenna forms. Designs can be easily fabricated from solid wire or tubular conductors and are (typically) very inexpensive. In this part we will start by considering the short dipole antenna to introduce the concepts, followed by an analysis of the more practical $\lambda/2$ dipole[1].

1 The short dipole

A short[2] wire of length $l \ll \lambda$ is positioned at the origin and orientated with the z-axis, as shown in Fig. 1. The current on the wire is assumed to be constant, and given by

$$\mathbf{I}(z) = \hat{a}_z I_0 \tag{1}$$

where I_0 is constant. In the analysis of antennas we are interested primarily in the electric and magnetic fields radiated by the currents flowing on the surface of the antenna. Before analysing radiation, it is useful to briefly review how the fields are expressed mathematically.

Electric and magnetic fields are *vector fields*—at every point in space, (x, y, z), the field has a magnitude and direction. For example, in rectangular coordinates the electric field can be decomposed into the weighted

[1]The short dipole is not used in practice, but is useful to understand the analysis process before moving onto more practical (and more complicated) antennas.

[2]This antenna goes by at least three names in the literature: the *short* dipole, the *infinitesimal* dipole, and the *Hertzian* dipole.

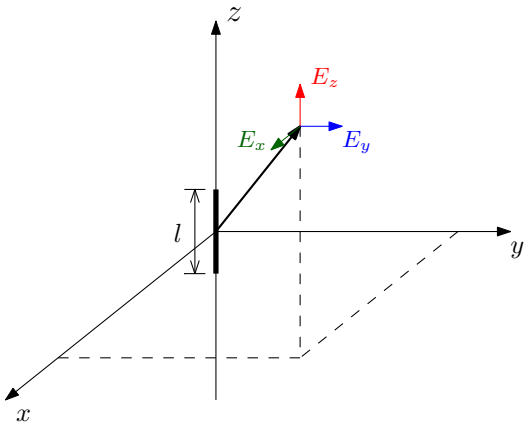

(a)

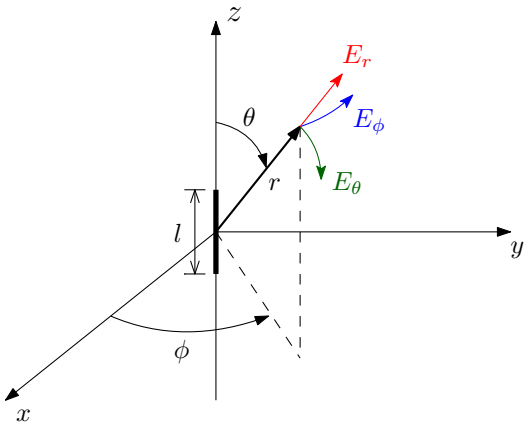

(b)

Fig. 1: Electric field components radiated from a short dipole in (a) a rectangular coordinate system and (b) a spherical coordinate system. Adapted from [1, p. 113].

summation of three orthogonal unit vectors, $\hat{a}_x$, $\hat{a}_y$ and $\hat{a}_z$, namely

$$\mathbf{E}(x,y,z) = \hat{a}_x E_x(x,y,z) + \hat{a}_y E_y(x,y,z) + \hat{a}_z E_z(x,y,z). \tag{2}$$

A sketch of the electric field in rectangular coordinates is shown in Fig. 1(a). However, when considering antennas it is usually more convenient use spherical coordinates, as shown in Fig. 1(b). In this case the electric field can be expressed as

$$\mathbf{E}(r,\theta,\phi) = \hat{a}_r E_r(r,\theta,\phi) + \hat{a}_\theta E_\theta(r,\theta,\phi) + \hat{a}_\phi E_\phi(r,\theta,\phi) \tag{3}$$

where $\hat{a}_r$, $\hat{a}_\theta$, and $\hat{a}_\phi$ are the spherical coordinate unit vectors. Similar expressions can also be written for the magnetic fields.

1.1 Fields radiated by a short dipole

In spherical coordinates, the fields radiated by a short dipole carrying current I_0 and orientated along the z-axis, are[3]

$$H_r = 0 \tag{4}$$
$$H_\theta = 0 \tag{5}$$
$$H_\phi = j\frac{kI_0 l \sin\theta}{4\pi r}\left[1 + \frac{1}{jkr}\right]e^{-jkr} \tag{6}$$
$$E_r = \eta\frac{I_0 l \cos\theta}{2\pi r^2}\left[1 + \frac{1}{jkr}\right]e^{-jkr} \tag{7}$$
$$E_\theta = \eta\frac{kI_0 l \sin\theta}{4\pi r}\left[1 + \frac{1}{jkr} - \frac{1}{(kr)^2}\right]e^{-jkr} \tag{8}$$
$$E_\phi = 0 \tag{9}$$

where k is the wave-number ($k = \frac{2\pi}{\lambda}$) and η is the intrinsic impedance of free-space ($\eta \approx 377\ \Omega$). Visualising the field created by these components is difficult, so in the following sections we will make simplifying approximations to focus on the fields radiated at a large distance from the antenna (*far-field*); and the fields in the region very close to the antenna (*near-field*).

1.2 Field regions

Fig. 2 identifies three regions around an antenna: the *reactive near-field*; the *radiating near-field*; and the *far-field*. In general, the field has distinct properties in each, i.e., different terms in (4)–(9) will dominate in each region. Approximate expressions for the boundaries between the regions are [2, p. 31]:

$$\begin{aligned}
\text{Reactive near-field:} &\qquad R < 0.62\sqrt{D^3/\lambda} \\
\text{Radiating near-field:} &\qquad 0.62\sqrt{D^3/\lambda} < R < \frac{2D^2}{\lambda} \\
\text{Far-field:} &\qquad R > \frac{2D^2}{\lambda}
\end{aligned}$$

where D is the largest physical dimension of the antenna (consequently, these expressions are *not* valid for a short dipole). It should also be noted there is not an abrupt change in the field when crossing any of these 'virtual' boundaries.

[3]The derivation of these equations from Maxwell's Equations can be found in any antenna textbook, e.g., [1, pp. 100–103], [2, pp. 16–24], [3, pp. 19–25].

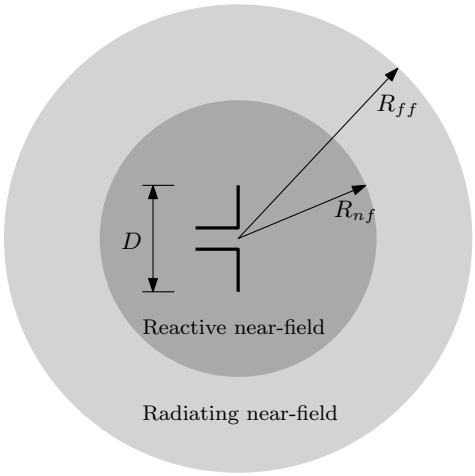

Fig. 2: Field regions around an arbitrary antenna, with largest physical dimension, D. Adapted from [1, p. 22].

1.3 Far-field

In far-field of a short dipole, where $r \gg \lambda$, (4)–(9) can be simplified, as any terms proportional to $\frac{1}{r^2}$ and $\frac{1}{r^3}$ will vanish, leading to,

$$H_\phi \simeq j\frac{kI_0le^{-jkr}}{4\pi r}\sin\theta \tag{10}$$

$$E_r \simeq E_\phi = H_r = H_\theta = 0 \tag{11}$$

$$E_\theta \simeq j\eta\frac{kI_0le^{-jkr}}{4\pi r}\sin\theta \tag{12}$$

We often separate out the terms, e.g., for E_θ,

$$E_\theta = \underbrace{C}_{\text{constants}} \times \underbrace{\frac{1}{r}}_{\text{amplitude term}} \times \underbrace{e^{-jkr}}_{\text{phase term}} \times \underbrace{f(\theta,\phi)}_{\text{field pattern}} \tag{13}$$

where, for the short dipole,

$$C = j\eta\frac{kI_0l}{4\pi} \tag{14}$$

$$f(\theta,\phi) = \sin\theta. \tag{15}$$

Note that the field pattern is only a function of the angles θ and ϕ, and for the short dipole it **only** depends on θ—what does this imply?

From (10) and (12) we observe that in the far-field the electric and magnetic field components are:

- orthogonal (perpendicular) to each other;
- in phase;

- transverse to the direction of propagation (i.e., $H_r = E_r = 0$); and
- $E_\theta = \eta H_\phi$
- exhibit a $\frac{1}{r}$ distance dependency.

In the far-field region, the fields radiated from a short-dipole thus form a *transverse electromagnetic* (TEM) wave.

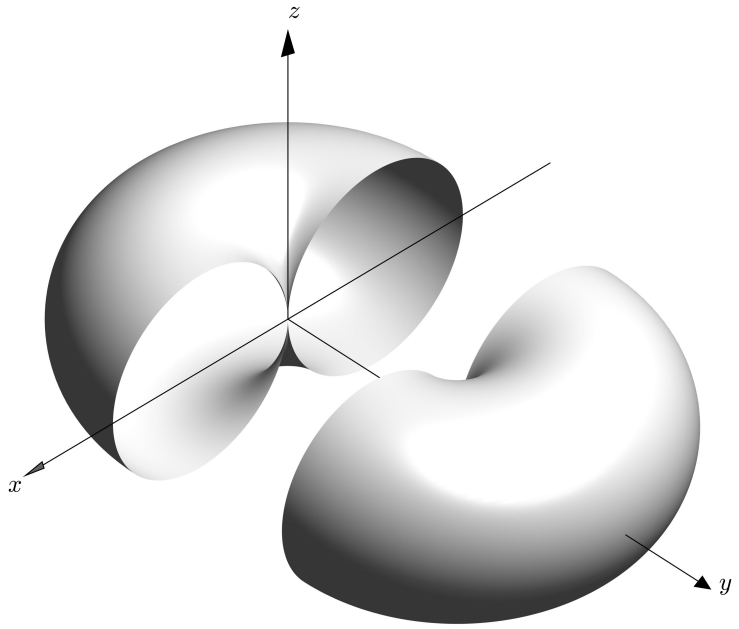

Fig. 3: Nominal E_θ field pattern for a short-dipole antenna measured in the far-field region. Adapted from [1, p. 31].

The three-dimensional far-field pattern, i.e., $f(\theta, \phi)$ of a short dipole antenna (located at the origin and orientated along the z-axis) is shown in Fig. 3. Note that this is an 'exploded' view. Fig. 4(a) and (b) show the same field pattern in the two-dimensional *elevation* and *azimuth* planes respectively. Some qualitative observations:

- The three-dimensional pattern is somewhat torus shaped;
- Maximum radiation occurs at $\theta = 90°$ for all values of ϕ;
- No radiation occurs at $\theta = 0°$, i.e., along the z-axis;
- The fields are *independent* of ϕ, i.e., the pattern in the azimuthal plane is a circle (this is not surprising as the geometry is rotationally symmetric); and
- The 3-dB *beamwidth* (representing half-power) is 90°.

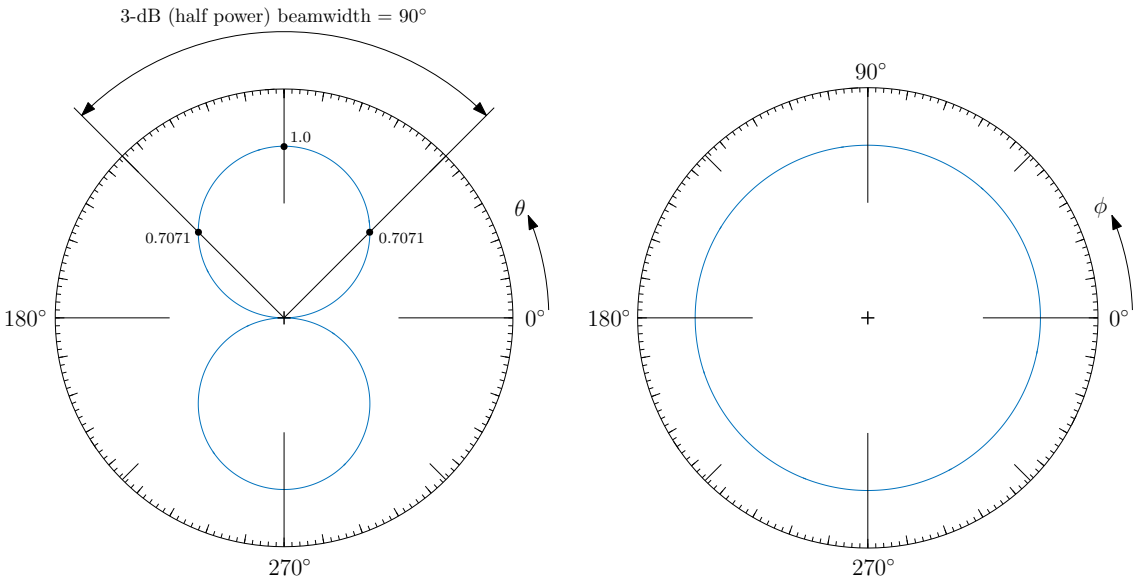

(a) (b)

Fig. 4: Far-field E_θ field patterns, $f(\theta, \phi)$, in the (a) elevation plane; and (b) azimuth plane.

1.4 Antenna gain

The *gain* of antenna is a important parameter that often used in link-budget analysis and is typically measured in dBi—dB relative to an isotropic source[4]. The antenna gain provides a measure of how much it concentrates energy in particular directions, and in this section we will outline how the gain is related to the radiation pattern:

1. The *directivity* of an antenna is defined as the ratio of its maximum radiation intensity, U, over that of an isotropic source, U_0, i.e.,

$$D = \frac{\max U}{U_0}. \tag{16}$$

   The directivity is a unit-less quantity.

2. The radiation intensity, U, can be expressed as

$$U = r^2 W_{rad} \tag{17}$$

   where W_rad is the radiation intensity measured in W/m^2, and is given by the Poynting vector of the far-fields,

$$W_{rad} = \frac{1}{2}\Re\left[\mathbf{E} \times \mathbf{H}^*\right]. \tag{18}$$

[4]An isotropic source radiates equally well in all directions, i.e., the field pattern is independent of both θ **and** ϕ. It does not exist, but is a useful concept.

3. It can be shown that the radiation intensity of an *isotropic source* is

$$U_0 = \frac{P_{rad}}{4\pi} \tag{19}$$

leading to the following expression for the directivity

$$D = 4\pi \frac{\max U}{P_{rad}}. \tag{20}$$

4. For a lossless antenna, the gain is equal to the directivity, however in reality, conduction losses on the metal will reduce the radiated power, leading to

$$g = e_t D \tag{21}$$

where $e_t \leq 1$ is the antenna *efficiency* (dimensionless) and accounts for the conduction loss.

The gain relative to a dipole, dBd, is also a commonly used parameter. How can we simply convert between dBi and dBd?

1.5 Near-field

In the near field regions around a short dipole, the fields are dominated by the terms in (4)–(9) proportional to $1/r^2$ and $1/r^3$, i.e.,

$$H_\phi \simeq \frac{kI_0 l e^{-jkr}}{4\pi} \frac{1}{r^2} \sin\theta \tag{22}$$

$$E_r \simeq -j\eta \frac{I_0 l}{2\pi k} \frac{1}{r^3} \cos\theta \tag{23}$$

$$E_\theta \simeq -j\eta \frac{I_0 l \sin\theta}{4\pi k} \frac{1}{r^3} \sin\theta \tag{24}$$

$$E_\phi = H_\theta = H_r = 0 \tag{25}$$

For radio system design we are typically not interested in the near-field patterns, however, there can be significant consequences to the far-field pattern if we place objects (particularly conductors) in the near-field.

An interesting consequence of (22)–(25) is that the average power in the near-field of an infinitesimal dipole antenna is zero! It is important

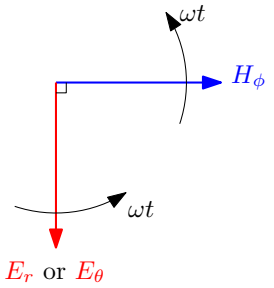

Fig. 5: Phasor diagram showing the relationship between the E and H field components in the near field.

to remember that the vector fields in (4)–(9) are assumed to be in time-harmonic form, e.g.,

$$\mathcal{E}(t) = \Re\left(\mathbf{E}\, e^{j\omega t}\right) \tag{26}$$

$$\mathcal{H}(t) = \Re\left(\mathbf{H}\, e^{j\omega t}\right). \tag{27}$$

We can view the vector fields $\mathcal{E}(t)$ and $\mathcal{H}(t)$ as the projection onto the real-axis of the vectors $\mathbf{E}$ and $\mathbf{H}$ rotating at ωt—this is the *phasor* representation and can be very helpful in visualising the relationships between vector quantities.

Fig. 5 shows a phasor diagram of the E_r, E_θ and H_ϕ components, as given by (6), (7), and (8). At this stage we are not interested in the magnitudes of the components, but rather their relative phase—specifically, we observe that the electric field vectors are offset in time from the magnetic field vector by 90°. This offset arises from the presence of j in (7) and (8), which is not present in (6).

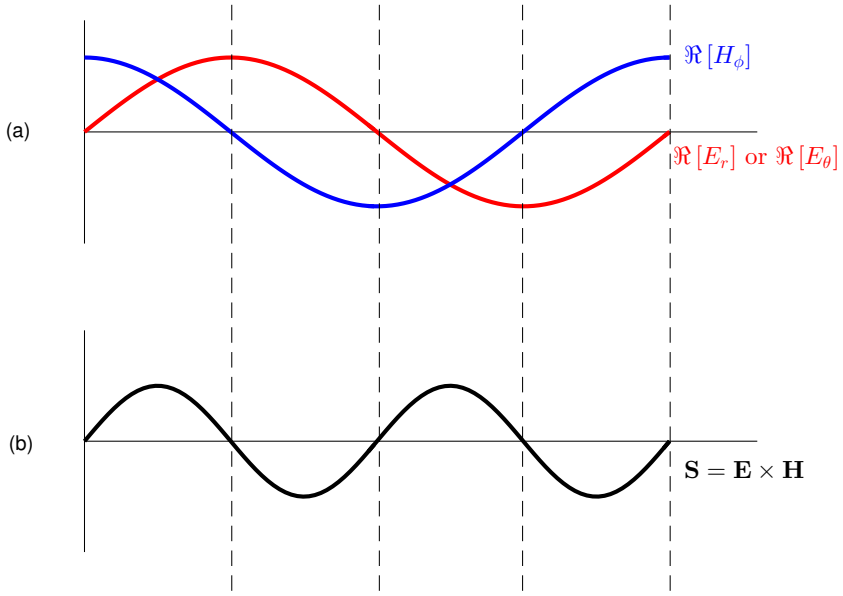

Fig. 6: (a) Projection of the E and H phasors onto the real-axis; (b) $\hat{a}_\theta$ and $\hat{a}_r$ components of the instantaneous Poynting vector.

Fig. 6(a) shows the projection of the phasors onto the real-axis, where this 90° offset is also apparent. It can be shown[5] that the *instantaneous*

[5]Mathematically, the *instantaneous* Poynting vector can be expressed

$$\begin{aligned}
\mathcal{W}(t) &= \mathcal{E}(t) \times \mathcal{H}(t) \\
&= \Re\left[\hat{a}_r E_r e^{j\omega t} + \hat{a}_\theta E_\theta e^{j\omega t}\right] \times \Re\left[\hat{a}_\phi H_\phi e^{j\omega t}\right] \\
&= \hat{a}_r \Re\left[E_r e^{j\omega t}\right] \times \hat{a}_\phi \Re\left[H_\phi e^{j\omega t}\right] + \hat{a}_\theta \Re\left[E_\theta e^{j\omega t}\right] \times \hat{a}_\phi \Re\left[H_\phi e^{j\omega t}\right] \\
&= \hat{a}_\theta \Re\left[E_r e^{j\omega t}\right] \Re\left[H_\phi e^{j\omega t}\right] + \hat{a}_r \Re\left[E_\theta e^{j\omega t}\right] \Re\left[H_\phi e^{j\omega t}\right].
\end{aligned} \tag{28}$$

Poynting vector is proportional to the product the field quantities plotted in Fig. 6(a), and this result is depicted in Fig. 6(b). The power in the near field region thus flows outward for a quarter-cycle, then inwards for a quarter-cycle (which is then repeated), leading to **no net radiation of power** in the near-field. Power can be coupled out if a receiving antenna is placed in the near-field (e.g., wireless power transfer) but in this case the analysis would need to consider the transmitting and receiving antennas as a single coupled system. Such an analysis can be complicated as it requires very accurate modelling of the surface currents which are sensitive to the geometry.

2 Finite-length dipoles

For the infinitesimal dipole we assumed the length was much smaller than the wavelength and thus the current can be approximated as constant. On an arbitrary "long" dipole this assumption does not hold. Determining the actual current distribution on a wire antenna can be complicated, and for complex shapes often requires a numerical solution. However, once the current distribution is found, the radiation pattern of an arbitrary wire antenna can be determined by subdividing the length into a number of short dipoles of length $\Delta z'$ and applying superposition. As the number of subdivisions is increased, each short dipole approaches a length dz'.

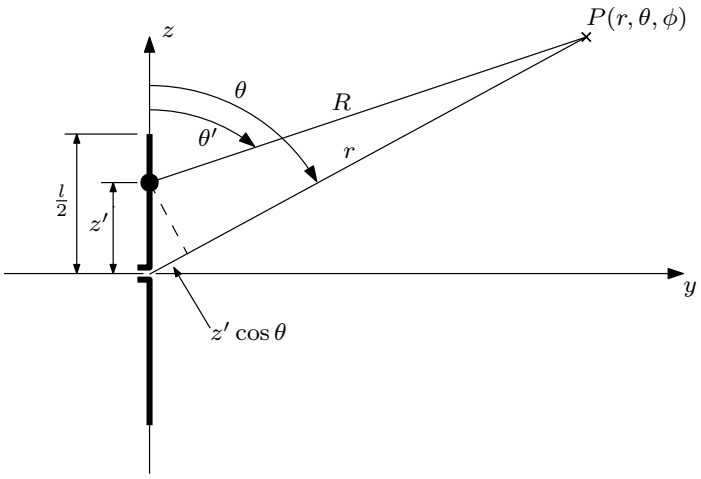

Fig. 7: Far-field approximation for a "long" dipole. Adapted from [1, p. 113].

Fig. 7 shows a "long" wire dipole antenna, orientated along the z-axis with the feed located at the origin. To compute the E_θ field in the far-field from this antenna, we will start by considering the field radiated from a short dipole that is located at z' from the origin. This is given by

$$dE_\theta \simeq j\eta \frac{kI(z')e^{-jkR}}{4\pi R} \sin\theta \, dz' \tag{29}$$

The two terms in (28) have a similar form, i.e., the multiplication of the real-projection of the E and H phasors, leading to the representation sketched in Fig. 6(b).

where R is the distance from the dipole at z' to a point P in the far-field, Note that R is not the same as r, which is the distance from the origin to P. A far-field approximation is used to simplify (29):

$$R \simeq r - z' \cos\theta \qquad \text{for phase terms} \tag{30}$$

$$R \simeq r \qquad \text{for amplitude terms} \tag{31}$$

leading to

$$dE_\theta \simeq j\eta \frac{kI(z')e^{-jkr}}{4\pi r} \sin\theta e^{+jkz'\cos\theta}\, dz'. \tag{32}$$

The total E_θ field is thus the summation of all the dz' elements from $-\frac{l}{2}$ to $\frac{l}{2}$, and in the limit, this summation becomes an integration,

$$\begin{aligned} E_\theta &\simeq \int_{-\frac{l}{2}}^{\frac{l}{2}} dE_\theta \\ &\simeq j\eta \frac{ke^{-jkr}}{4\pi r} \sin\theta \left[\int_{-\frac{l}{2}}^{\frac{l}{2}} I(z') e^{jkz'\cos\theta} dz' \right]. \end{aligned} \tag{33}$$

It should be noted that the term outside the brackets is simply the E_θ field radiated by a unit-current short dipole located at the origin; while the term in the brackets is a function of the current distribution on the antenna.

3 $\lambda/2$ dipole

The current on a $\lambda/2$ dipole can be approximated as

$$I(z) = \hat{a}_z I_0 \sin\left[k\left(\frac{l}{2} - z\right)\right] \tag{34}$$

where I_0 is the nominal maximum current. As shown in Fig. 8(a), it is assumed the maximum current occurs at the antenna terminals—in practice, this will drop slightly around the connection point, as shown in Fig. 8(b)—and goes to zero at the ends of the antenna. These deviations generally do not have a large impact on the accuracy of the radiation patterns. The radiation pattern is determined by essentially summing up small sections of current (i.e., integrating), and this has an averaging/smoothing effect.

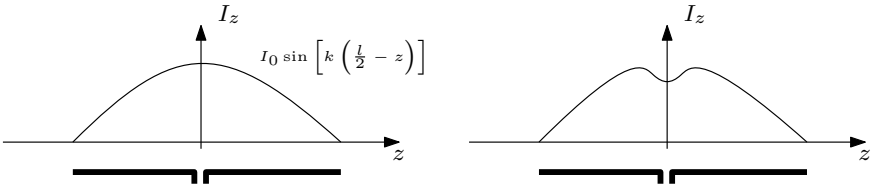

(a) (b)

Fig. 8: Current distribution on a $\lambda/2$ dipole: (a) ideal case; (b) real case with a drop in current around the connection point.

3.1 Field patterns (far-field)

Substituting (34) into (33) (and after some manipulations[6]) leads to general expressions for a dipole of length l,

$$E_\theta \simeq j\eta \frac{I_0 e^{-jkr}}{2\pi r} \left[\frac{\cos\left(\frac{kl}{2}\cos\theta\right) - \cos\left(\frac{kl}{2}\right)}{\sin\theta} \right] \tag{36}$$

$$H_\phi \simeq j \frac{I_0 e^{-jkr}}{2\pi r} \left[\frac{\cos\left(\frac{kl}{2}\cos\theta\right) - \cos\left(\frac{kl}{2}\right)}{\sin\theta} \right]. \tag{37}$$

For a dipole with $l = \lambda/2$, these expressions simplify to

$$E_\theta \simeq j\eta \frac{I_0 e^{-jkr}}{2\pi r} \left[\frac{\cos\left(\frac{\pi}{2}\cos\theta\right)}{\sin\theta} \right] = \eta H_\phi \tag{38}$$

$$H_\phi \simeq j \frac{I_0 e^{-jkr}}{2\pi r} \left[\frac{\cos\left(\frac{\pi}{2}\cos\theta\right)}{\sin\theta} \right]. \tag{39}$$

Similar to the short dipole, the field pattern term (which only depends on θ and ϕ) can be separated out,

$$f(\theta, \phi) = \frac{\cos\left(\frac{\pi}{2}\cos\theta\right)}{\sin\theta}. \tag{40}$$

The field pattern alsodoes not depend on ϕ, i.e., the radiation pattern in the azimuth plane is a circle (due to symmetry).

Note that the *magnitudes* of the electric and magnetic fields only differ by the factor η, representing the impedance of free-space. Similar to the short-dipole, the fields in the far-field region are TEM. While (38) and (39) appear to be more complicated than the expressions for the short dipole, the radiation patterns turns out to be quite similar, as shown in Fig. 9 which compares a polar plot (in the elevation plane) of a short dipole (15) with a $\lambda/2$ dipole (40). The 3-dB beamwidth of the $\lambda/2$ dipole is 78°.

3.2 Input impedance

The impedance seen looking into the terminals of an antenna is an important parameter that must be known to match the antenna to transmission line, thus providing maximum power transfer. The input impedance can be divided into two components:

$$Z_{in} = R_{in} + jX_{in}. \tag{41}$$

- The *input resistance*, R_{in}, represents dissipation of power—which occurs in two ways: radiation, i.e., power that leaves the antenna and does not return; and Ohmic losses, i.e., power lost by heating,

$$R_{in} = R_{Rad.} + R_{Ohmic}. \tag{42}$$

[6]Including use of the integral

$$\int e^{\alpha x} \sin(\beta x + \gamma)\, dx = \frac{e^{\alpha x}}{\alpha^2 + \beta^2} \left[\alpha \sin(\beta x + \gamma) - \beta \cos(\beta x + \gamma)\right] \tag{35}$$

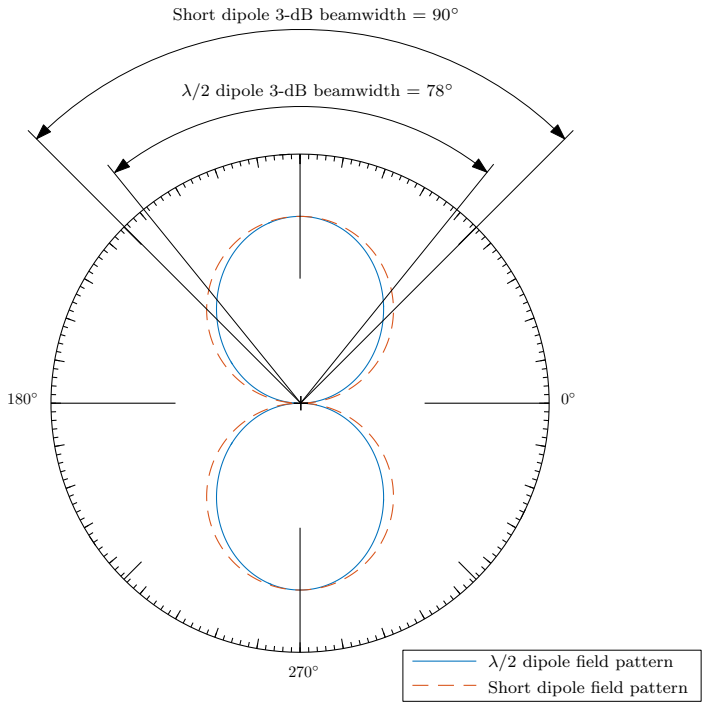

Fig. 9: Elevation plane field pattern for $\lambda/2$ dipole compared with a short dipole.

Typically the power lost to heating is small compared to the radiated power: this is quantified by the *radiation efficiency*, e_r which is the ratio of the radiation resistance, $R_{Rad.}$ to R_{in}, i.e.,

$$e_r = \frac{R_{Rad.}}{R_{Rad.} + R_{Ohmic}} \tag{43}$$

and is often expressed as a percentage. Generally, $R_{Rad.}$ can be found relatively easily by equating the input power (since we know the current at the input terminals) with the expression for the power radiated in the far field, which is computed by taking a surface integral of the Poynting vector over a sphere that encompasses the antenna. Similarly, R_{Ohmic} can be determined using expressions for a conductor in an AC field. For a $\lambda/2$ dipole $R_{in} \approx 73\ \Omega$ and typically $e_r > 90\%$.

- The *input reactance*, X_{in}, represents the (reactive) power stored in the near-field. Calculating X_{in} requires very accurate expressions for the current excited on the antenna (often to a higher degree of precision than that required to find the radiated fields). Accordingly, the reactance also depends on the thickness of the wire. It is usually not possible to find closed form expressions for X_{in}, and numerical electromagnetic solutions are typically required.

The input impedance also depends on how the transmission line feed is connected (this can usually only be included using numerical approaches).

3.3 Longer dipoles and bandwidth

Dipole antennas radiate best when the currents flowing along the physical length of the antenna establish a *resonant mode*. The current must go to zero at the ends of the antenna and hence resonant modes can be established when $l = \frac{n\lambda}{2}$, for $n = 1, 2, \ldots$. The case when $n = 1$ is the $\lambda/2$ dipole. The current distributions when $n = 2$ and $n = 3$ are sketched in Fig. 10(a) and (b). The corresponding radiation patterns in the elevation plane are shown in Fig. 11, and are computed using (36).

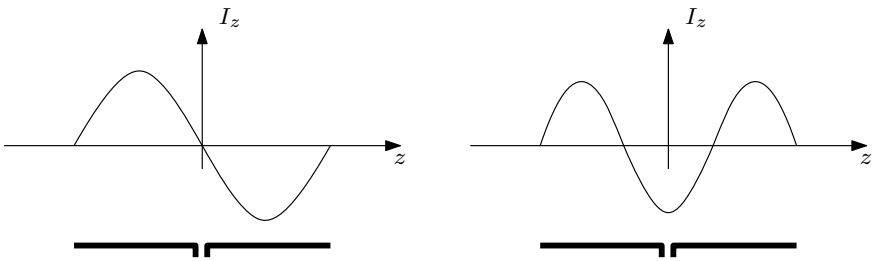

(a) (b)

Fig. 10: Current distribution on (a) λ dipole and (b) 1.5λ dipole.

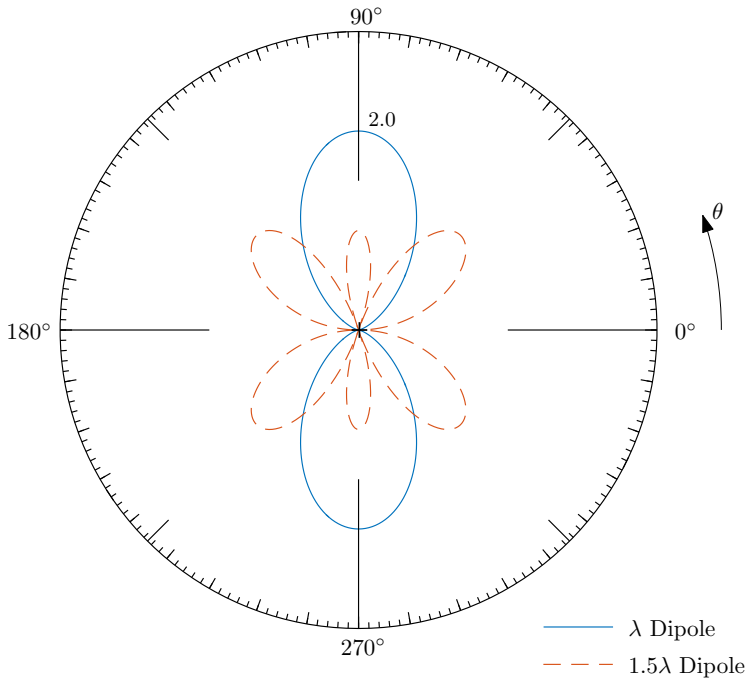

Fig. 11: Elevation plane field pattern comparing a λ dipole with a 1.5λ dipole.

Some observations to note are:

- The radiation pattern of the $3\lambda/2$ dipole has a number of side-lobes, which is typically an undesirable characteristic.
- The λ dipole would seem to be a reasonable antenna, with a higher gain (2.0) and correspondingly narrower beam-width than the $\lambda/2$ dipole.
- However, as shown in Fig. 10(a) at the feed connection point in the centre of the dipole, the current distribution required to achieve resonance goes to zero, i.e., Z_{in} approaches infinity, making it very difficult to match the antenna to the transmission line.

Resonant behaviour also implies dipole antennas will be *narrowband*. For example, Fig. 12 shows the magnitude of the reflection coefficient (also referred to as the S_{11}) as a function of frequency for a $\lambda/2$ dipole antenna designed for operation in the 2.48 GHz Wifi band. Some observations to note are:

- A reflection coefficient close to 0 dB (what is this in linear units?) indicates most of the energy is being *reflected*, and in the context of antennas, this means it is not being radiated!
- Conversely, a small reflection coefficient implies the energy is being radiated (or absorbed).

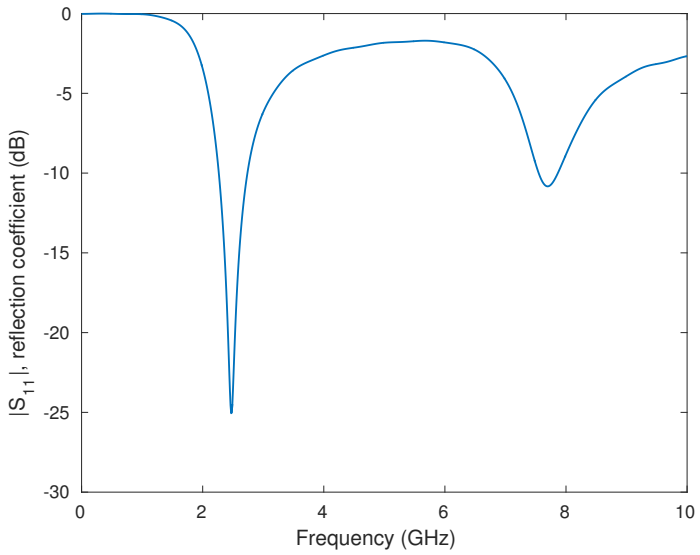

Fig. 12: Reflection coefficient for a $\lambda/2$ dipole antenna designed for operation at 2.48 GHz.

For the dipole in Fig. 12 we can observe there is only a relatively narrow band of frequencies where the reflection coefficient is below -15 dB, i.e.,

between 2.36–2.6 GHz (240 MHz bandwidth). This antenna would thus be suitable for a Wifi system in the 2.48 GHz band, but very unsuitable for the 5.8 GHz band! The secondary resonance around 7.8 GHz is when the electrical length of the antenna is approximately $3\lambda/2$—this is broader, but only achieves an S_{11} of -10 dB and with the unwanted radiation pattern in Fig. 11.

As an aside, the result in Fig. 12 was computed using CST Microwave Studio for a *realistic* dipole antenna, i.e., the wire was assumed to have some thickness (3 mm in this case) and a 3 mm gap for the feed was also assumed. Accordingly, to achieve resonance, the length of the antenna needed to be reduced from $l_{theory} = \lambda/2 = 60.5$ mm to $l_{opt.} = 55.7$ mm.

3.4 Baluns

In this section we consider the impact of connecting a dipole antenna to a transmission line. For example, Fig. 13 shows one way a dipole antenna can be physically attached to a coaxial transmission line. The coax inner conductor is connected directly to the left-arm of the dipole; while the right-arm is connected to the outer conductor of the coax. The left- and right-arms of the dipole are thus connected differently and the asymmetry can alter the current distribution on the antenna. In particular, while the current flowing on the left-arm of the dipole will be the same as the current on the inner conductor, i.e.,

$$I_1 = I_{d-left} \tag{44}$$

this does not hold for the right-arm of the dipole, as a current can also flow on the *outside surface* of the outer conductor, i.e.,

$$I_2 = I_{d-right} + I_3. \tag{45}$$

Effectively, this reduces the current flowing on the right-arm of the dipole, as depicted in Fig. 13, leading to an imbalance and thereby altering the radiation pattern and is undesirable characteristic. Specifically the radiation pattern due to the imbalance is often "squinted", i.e., the direction of maximum radiation is offset.

One solution to this problem is to use a *balun*. A balun is a relatively simple device that can be used to balance inherently unbalanced systems[7], by cancelling (or "choking") the outside/external current. Fig. 14(a) shows one popular balun configuration for a dipole antenna fed by a coaxial transmission line. It consists of a sleeve of metal, $\lambda/4$ in length, wrapped around the transmission line and electrically connected (i.e., shorted) to the outer conductor at one end.

Electrically, the sleeve and the outer conductor form another transmission line, where the equivalent circuit is shown in Fig. 14(b). The input impedance of this transmission line (looking in at the top end) is very large[8], ideally infinity, and thus the current flowing on the outside (I_3) will be eliminated, balancing the system.

[7] Hence the name: balun = *bal*anced to *un*balanced.

[8] The $\lambda/4$ length of transmission line transforms the short circuit into an open circuit.

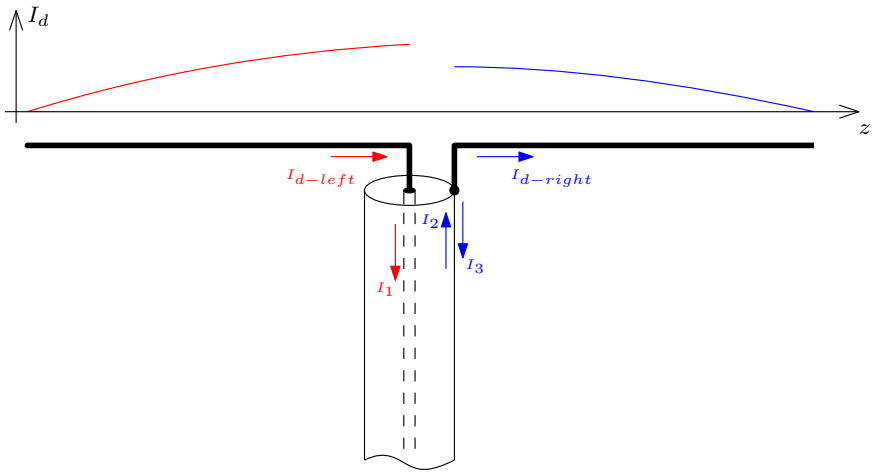

Fig. 13: "Direct" physical connection of a dipole antenna to a coaxial transmission line showing current distribution on the arms, leading to undesirable radiation characteristics.

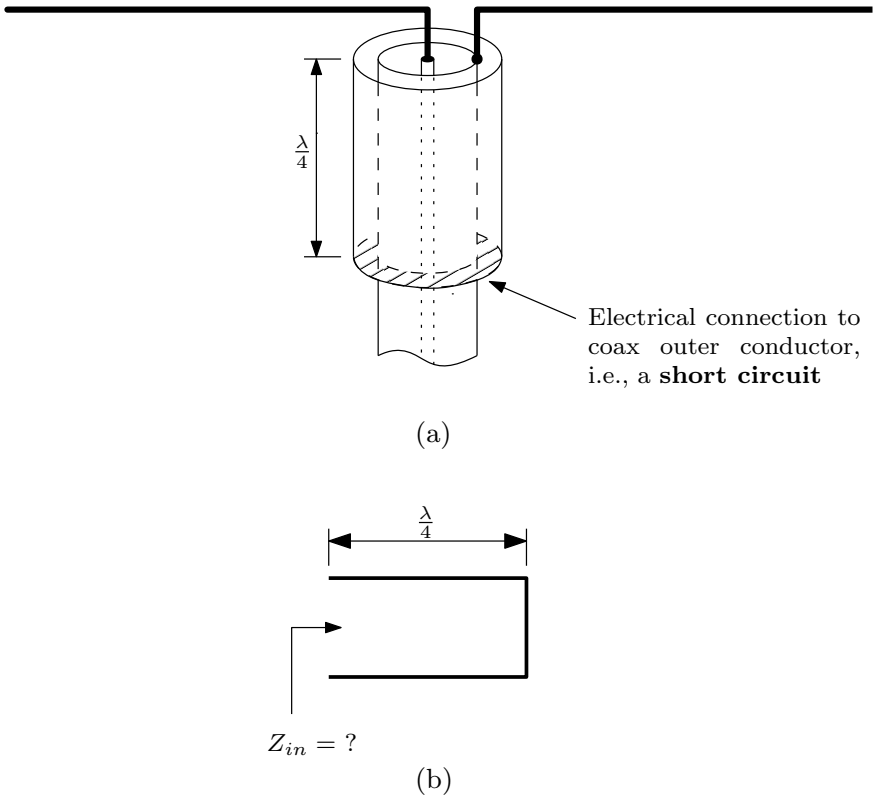

Fig. 14: (a) Balun constructed from a $\lambda/4$ sleeve of metal wrapped around the coaxial transmission line and shorted to the outer conductor; (b) equivalent transmission line circuit formed by the sleeve and outer conductor.

4 Corner reflector antennas

The radiation pattern of a dipole antenna in the azimuth plane is omni-directional, i.e., the antenna radiates (or receives) equally well in all directions. This is often a desirable characteristic of antennas that are mounted on mobile devices or where area coverage is required. However, there are often scenarios where a focused, directional beam is required (e.g., to reduce interference).

Reflectors can be placed behind an antenna to direct energy in a specific direction. A popular choice for dipole antennas is the corner reflector, as shown in Fig. 15. A vertically orientated dipole antenna is placed at a distance s from a corner that is formed by two perfect electrical conductor (PEC) sheets with width w and height h (the angle between these PEC sheets is α, and the antenna is located at $\frac{\alpha}{2}$). For this analysis we will assume the corner is infinite in extent, though measurements with $w \simeq 2s$ and $h \simeq 1.2l$ have found to agree well with the theory.

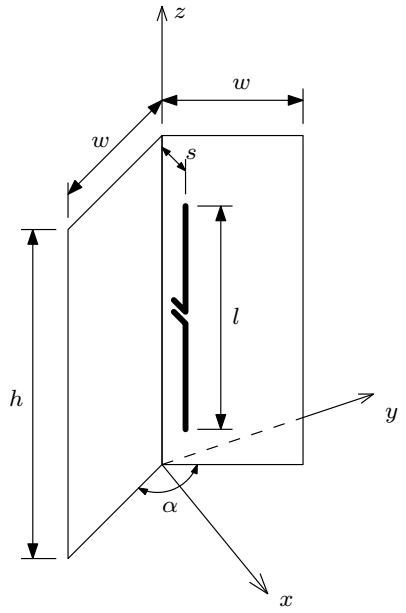

Fig. 15: Geometry of a corner reflector antenna.

Radiation pattern: The radiation pattern of a corner reflector can be found by considering the *images* created by reflecting the source antenna in the PEC sheets. For example, Fig. 16 shows that when $\alpha = 90°$ three images of the original dipole are formed. The far field pattern can be found by summing the electric fields from each of the three images with the electric field produced by the actual dipole. Note that due to symmetry, these are all located at a distance s from the origin. Also, due to the PEC boundary conditions[9] the fields radiated from image #2 and image #4 are **negative**, with respect to the field from the dipole.

[9]Specifically, that the tangential component of an electric field must be zero on a PEC

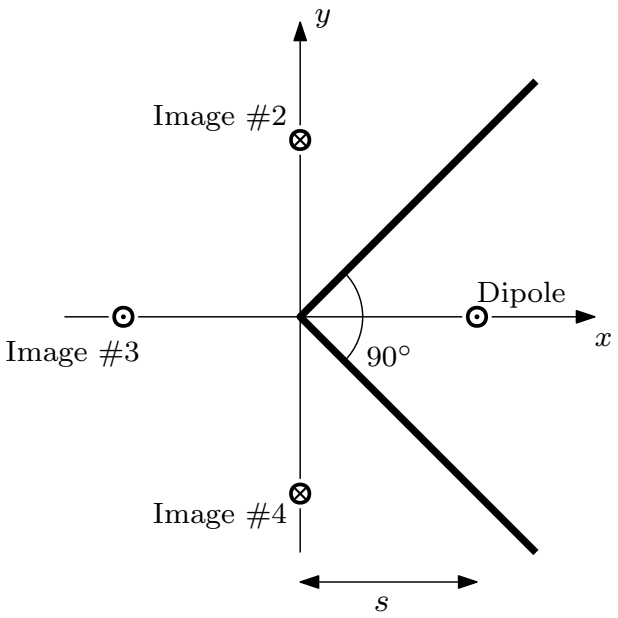

Fig. 16: Location of the images formed by a corner reflector. Note the change in sign for Images #2 and #4.

The total electric field can be expressed

$$E(r,\theta,\phi) = \underbrace{2\left[\cos(ks\sin\theta\cos\phi) - \cos(ks\sin\theta\sin\phi)\right]}_{\text{reflector gain}} f(\theta,\phi)\frac{e^{-jkr}}{r} \qquad (46)$$

where $f(\theta,\phi)$ is the field pattern of the dipole used, i.e., (15) for a short dipole, or (40) for a $\lambda/2$ dipole. The term of interest here is the *reflector gain*, as this suggests for certain values of s it is possible to increase the electric field strength by a (linear) factor of 4. What is the gain of this antenna in linear units? (and in dB?)

Fig. 17 shows the three-dimensional plot of the field pattern for a corner reflector with $s = \lambda/2$. The radiation pattern has a single main lobe and in this case the direction of maximum radiation is along the x-axis, as expected, given the position of the reflectors. Fig. 18 shows a polar plot of the corner reflector radiation pattern in the *azimuth* plane compared with the omni-directional pattern of a $\lambda/2$ dipole. The maximum of the corner reflector field pattern is 4 times that of the $\lambda/2$ dipole. However, the corner reflector will only radiate in the region between the PEC planes ($-45°$ – $45°$), i.e., the gain is only being increased by focusing the energy.

The radiation patterns in Fig. 17 and Fig. 18 are the *ideal* patterns assuming the PEC sheets forming the corner are infinite in extent. In reality, with finite metal sheets, some backlobes will be also be present due to diffraction around the edges of the sheet.

---

boundary.

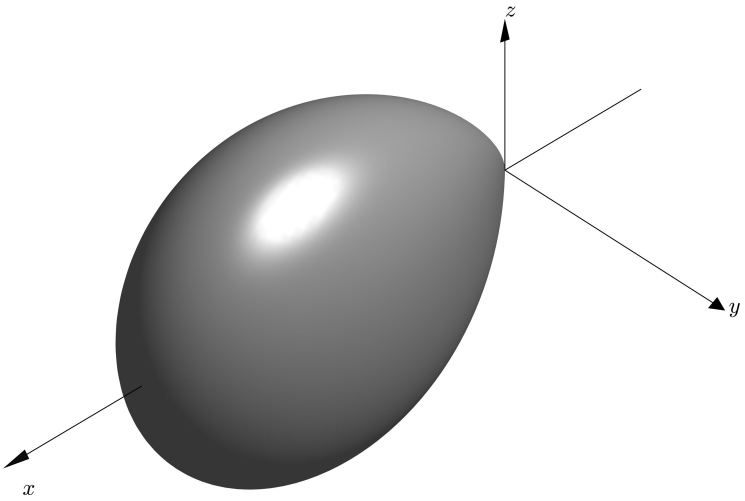

Fig. 17: Three-dimensional field pattern of a $\lambda/2$ corner reflector.

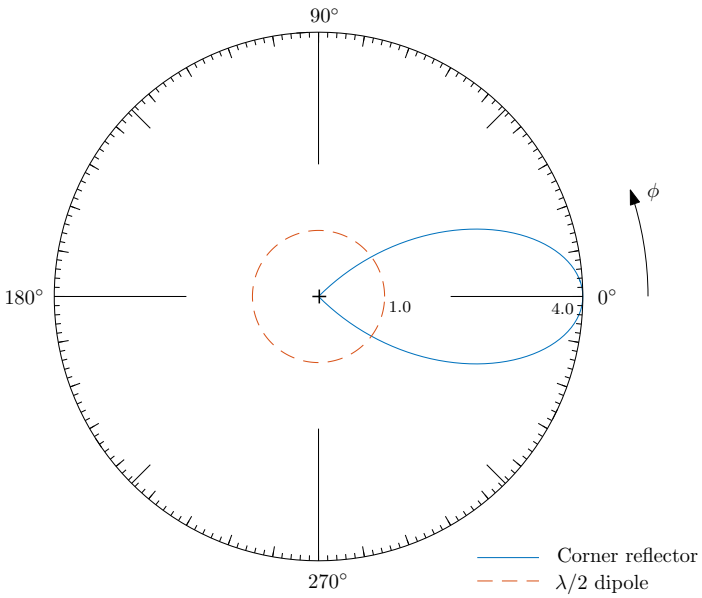

Fig. 18: Azimuth plane radiation pattern of a corner reflector compared with that of a $\lambda/2$ dipole.

Part B—Printed Antennas

Antennas fabricated using printed circuit board techniques were originally proposed in the 1950s and remain popular due to ease of construction, low profile and low manufacturing costs. In this part we will consider the basic rectangular patch antenna.

Patch antennas

The geometry of a rectangular patch antenna is shown in Fig. 19. The patch has dimensions $L \times W$ and is fed by a *microstrip* transmission line[10]. The patch is separated from the *infinite* ground plane by a dielectric substrate, with a known relative permittivity, ϵ_r, and with thickness h (typically $h \ll \lambda$). The length of the patch, L, is chosen so that a resonant mode can be established, i.e.,

$$L = 0.5\lambda_d = 0.5\frac{\lambda_0}{\sqrt{\epsilon_r}} \tag{47}$$

where λ_0 is the free-space wavelength and λ_d is the wavelength when propagating inside the dielectric substrate.

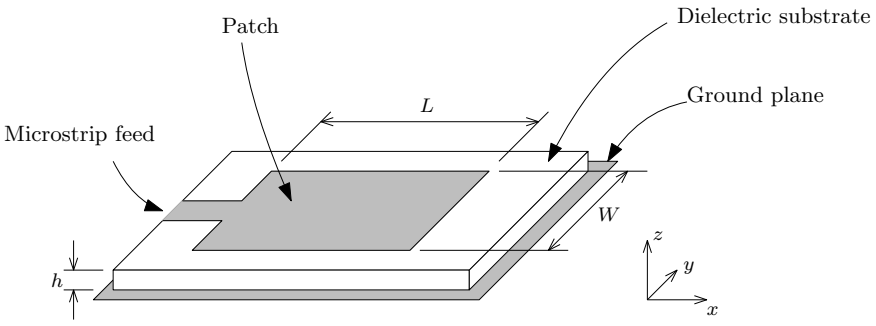

Fig. 19: Geometry of a rectangular patch antenna with microstrip line feed. Adapted from [2, p. 211].

The electric field distribution between the patch and the ground plane is shown in Fig. 20. The electric field is perpendicular to the ground plane and the patch, and is largest at the ends of the patch[11]. At the ends of the patch the *fringing fields* are exposed and are responsible for the radiation. In practise, the fringing fields at the ends of the patch also act to slightly *increase* the electrical length. Thus, often L needs to be reduced slightly, e.g.,

$$L \approx 0.49\lambda_d \tag{48}$$

to ensure resonant behaviour.

[10] The rectangular patch antenna can also be fed from a coaxial line passing through the dielectric substrate and ground-plane, but the results are very similar to the microstrip-fed patch.

[11] It is assumed these electric fields are constant across the width of the patch.

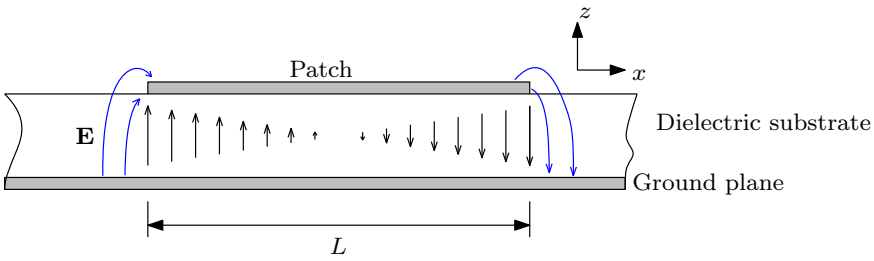

Fig. 20: Side view through a patch antenna showing the electric fields. Fringing fields are shown in blue. Adapted from [2, p. 211].

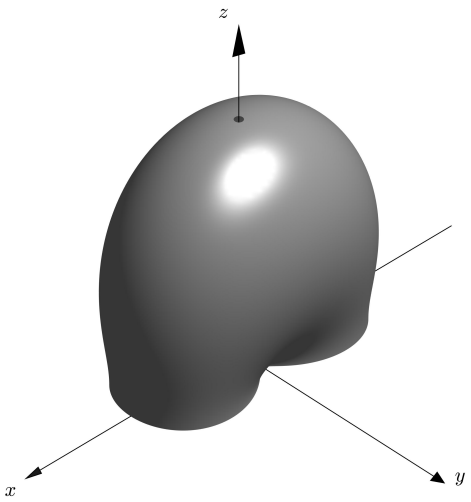

Fig. 21: Three dimensional radiation pattern from a patch antenna with geometry specified in Fig. 19.

Far-field pattern: An approximate expression for the radiation pattern is given by [2, p. 212]

$$f(\theta,\phi) = \frac{\sin\left(\frac{kW}{2}\sin\theta\sin\phi\right)}{\frac{kW}{2}\sin\theta\sin\phi}\cos\left(\frac{kL}{2}\sin\theta\cos\phi\right) \tag{49}$$

and a three-dimensional plot of this expression is shown in Fig. 21. The patch lies in the x–y plane and we observe that maximum radiation occurs in the z direction. Note that no fields exist below the infinite ground plane—in practise, a finite ground plane that is larger than the patch is required, but some fields will be diffracted, leading to small back-lobes. Fig. 22 shows two-dimensional elevation-plane cuts through the full 3D pattern—these plots are very common in antenna specifications and data-sheets as full 3D patterns can be difficult to measure and interpret quantitatively.

Input impedance: The patch width W is known to affect the input

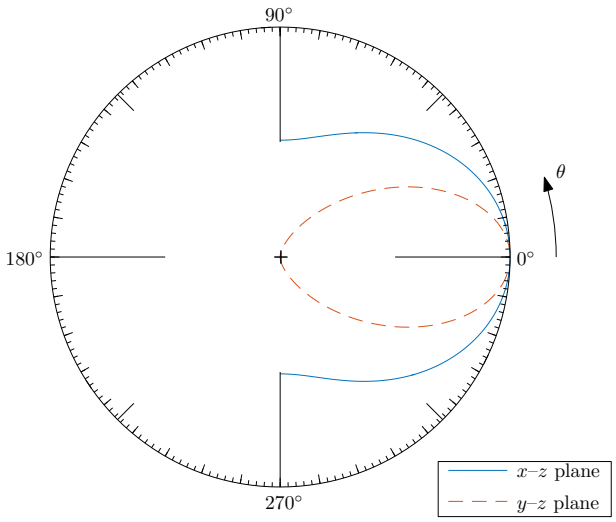

Fig. 22: Elevation plane patterns for a rectangular patch antenna.

impedance, and an approximate expression for Z_{in} is,

$$Z_{in} = 90\frac{\epsilon_r^2}{\epsilon_r - 1}\left(\frac{L}{W}\right)^2. \tag{50}$$

Note that this expression is purely real as the reactance is zero at resonance. From (50), we can choose W to match the patch to the characteristic impedance of the microstrip transmission line.

Bandwidth: The bandwidth of patch antennas tends to be small and is often a limiting factor when these are used for wideband systems. The bandwidth (as a fraction of the centre frequency) can be approximated as

$$B = 3.77\frac{\epsilon_r - 1}{\epsilon_r^2}\frac{W}{L}\frac{h}{\lambda}. \tag{51}$$

This indicates that bandwidth can be increased by changing the substrate properties, i.e., lowering ϵ_r and/or increasing h. However, this must be done with care as increasing h and decreasing ϵ_r will excite unwanted surface waves, which cause side-lobes and cross-polarisation.

References

[1] C. A. Balanis, *Antenna Theory: Analysis and Design*. New York: Harper & Row, 1982.

[2] W. L. Stutzman and G. A. Thiele, *Antenna Theory and Design*, 2nd ed. Hoboken, NJ: Wiley, 1998.

[3] R. E. Collin, *Antennas and Radiowave Propagation*. New York: McGraw-Hill, 1985.